Corner states in a second-order acoustic topological insulator as bound states in the continuum

Ze-Guo Chen,[1] Changqing Xu,[1] Rasha Al Jahdali,[1] Jun Mei,[2,*] and Ying Wu[1,†]

[1]*King Abdullah University of Science and Technology (KAUST), Division of Computer, Electrical and Mathematical Science and Engineering (CEMSE), Thuwal 23955-6900, Saudi Arabia*

[2]*Department of Physics, South China University of Technology, Guangzhou 510640, China*

(Received 11 January 2019; published 9 August 2019)

A second-order topological insulator is designed on a platform of a two-dimensional (2D) square lattice with all coupling coefficients having the same sign. Simulated results show the existence of two types of nontrivial corner states in this system, with one type being identified as bound states in the continuum (BIC). The non-BIC corner states are also found by surrounding a nontrivial sample by a trivial one, and interestingly, these perfectly confined corner states can be gradually delocalized and merge into edge states by tuning the intersystem coupling coefficient. Both BIC and non-BIC corner states originate from bulk dipole moments rather than quantized quadrupole moments, with the corresponding topological invariant being the 2D Zak phase. Full wave simulations based on realistic acoustic waveguide structures are demonstrated. Our proposal provides an experimentally feasible platform for the study of the interplay between BIC and a high-order topological insulator, and the evolution from corner states to edge states.

DOI: 10.1103/PhysRevB.100.075120

I. INTRODUCTION

Topology, a mathematical concept, was introduced to physics along with the discovery of the quantum Hall effect [1–3]. This concept has attracted growing attention accompanying the developments of various topological effects, including the quantum spin Hall effect [4,5] and the quantum valley Hall effect [6,7]. Recently, some other topological materials, including Floquet topological insulators and topological crystalline insulators, were proposed and studied [8–12]. A key characteristic of a topological material is the existence of gapless edge states on its boundary, which are immune to defects and impurities as long as the corresponding symmetry is preserved, leading to robust unidirectional transport of electrons without backscattering. Thus, it had been believed that a d-dimensional nontrivial material should host $(d-1)$-dimensional gapless edge states on its boundary. This position was held until very recently, when so-called higher-order topological insulators (HOTIs) were discovered [13–17]. It turns out that a d-dimensional topological insulator does not necessarily possess a $(d-1)$-dimensional edge state. Alternatively, it can support $(d-n)$-dimensional boundary states. For example, a two-dimensional (2D) second-order topological insulator does not exhibit one-dimensional (1D) gapless edge states, but it hosts nontrivial zero-dimensional (0D) corner states. Several tight-binding models, considering quantized quadrupole and octupole moments, have been proposed as candidates for HOTIs [13,18], and attention was soon extended to the platforms of classical waves including electromagnetic [19–21], acoustic [22–24], and mechanical waves [25] due to their flexibility in adjusting the geometries and potentials.

As another emerging interesting topic in wave propagation, bound states in continuum (BIC) refer to localized and nonradiative modes whose frequencies are embedded in the continuous spectrum of radiating waves [26]. The physical mechanism behind this somewhat counterintuitive phenomenon is diverse, and the prohibited radiation may be attributed to symmetry mismatch [27] or decoupling through separability [28], or to an interference effect between multiple radiation channels [29,30]. The ultrahigh-quality factor of the BIC is unique and highly desirable for large-area high-power applications including lasing [31–33], sensing [34,35], filtering [36], and nonlinearity enhancement [26].

In this work, we study both the topologically nontrivial corner states and the BIC. We demonstrate that these two seemingly unrelated topics could be combined naturally in a simple 2D system. We focus on a special kind of corner states that are simultaneously BIC and nontrivial boundary states of a HOTI. The physical properties of the corner states are studied and explored in realistic acoustic waveguide structures both analytically from a tight-binding model and numerically by full wave simulations. Interestingly, in the same platform we also identify the existence of the non-BIC corner states of a second-order HOTI. The evolution and transition between these two types of corners states can be realized by tuning the intersystem coupling coefficient. Different from the previously reported works [13,25], the proposed 2D system in our work does not rely on the introduction of a negative hopping amplitude for the realization of a HOTI. Although both of them are characterized by the 2D Zak phase, their origins are intrinsically different: the corner states studied here are strongly related to the bulk dipole moments [21], while the

*phjunmei@scut.edu.cn
†ying.wu@kaust.edu.sa

corner states reported in Ref. [13] are due to the quantized quadruple moments.

II. DESIGN AND MODEL OF THE SECOND-ORDER ACOUSTIC TOPOLOGICAL INSULATOR

The acoustic crystal (AC) considered here is a 2D square lattice composed of rings and waveguides filled with air. As illustrated in Fig. 1(a), the unit cell with a lattice constant $a = 4$ m contains four identical hollow rings with inner and outer radii as $r_0 = 0.35$ m and $r_1 = 0.5$ m. Each ring is connected to its nearest neighbors by four rectangular waveguides. The acoustic wave propagates inside the network of these rings and waveguides. Its pressure field φ satisfies the governing equation $[\nabla^2 + \omega^2/c^2]\varphi(\vec{r}, \omega) = 0$, where c is the sound velocity in air, and the boundaries of the rings and waveguides are treated as hard walls: $\mathbf{n} \cdot \nabla\varphi = 0$, where $\mathbf{n}$ is the normal vector of the boundaries.

The adjacent rings are correlated only through the waveguides, suggesting that the rings and waveguides effectively act as sites and coupling, respectively, in the picture of tight binding [37]. In the low-frequency regime, the hopping amplitude (i.e., the coupling coefficient) between two neighboring rings is proportional to the width of the waveguides, because only fundamental modes can survive inside the waveguides. The intracell and intercell hopping amplitudes are denoted as w and v, respectively, and they can be realized in a realistic AC structure by waveguides with different widths [38,39]. For such an AC system, in the momentum space, the Hamiltonian can be written as

$$H(k) = \begin{pmatrix} \varepsilon_s & -w - ve^{-ik_x a} & -w - ve^{-ik_y a} & 0 \\ -w - ve^{ik_x a} & \varepsilon_s & 0 & -w - ve^{-ik_y a} \\ -w - ve^{ik_y a} & 0 & \varepsilon_s & -w - ve^{-ik_x a} \\ 0 & -w - ve^{ik_y a} & -w - ve^{ik_x a} & \varepsilon_s \end{pmatrix}, \tag{1}$$

where ε_s is the onsite energy (or eigenfrequency) of each ring, and k_x, k_y is the Bloch wave vector. We introduce a negative sign in front of both w and v so that the lowest-energy mode (in the long-wavelength limit) is symmetric, which is widely adopted in solid-state physics [40]. Let us consider two different configurations of the unit cells. Configuration A has the hopping amplitude $w = 5v$, and configuration B has $v = 5w$. As shown in Fig. 1(a), these two configurations can be simulated in AC systems by setting the corresponding waveguide widths as $d_w = 0.05$ m and $d_v = 0.01$ m (for configuration A), and $d_w = 0.01$ m and $d_v = 0.05$ m (for configuration B), respectively. Details can be found in Appendixes A and B. Obviously, periodically repeating these unit cells in the 2D space would eventually give rise to two identical ACs that share the same band structure. Both the simulation results obtained from the finite-element method (black dots) and the calculation results obtained by the tight-binding model (red curves) are plotted in Fig. 1(b), and they agree with each other very well. Detailed fitting parameters for the tight-binding model are given in Appendix A.

Although configurations A ($w = 5v$) and B ($v = 5w$) share the identical band structure, they are topologically inequivalent. Inspired by the well-known 1D Su-Schrieffer-Heeger (SSH) model, one can simply guess that at the critical point $w = v$ [41], where the band gap closes, topological phase transition occurs. To rigorously characterize the topological phase transition, we need to calculate the corresponding topological index or invariant. Here the relevant topological invariant is the 2D Zak phase or 2D polarization, which is defined as the integral of the Berry connection through [42]

$$\mathbf{P} = \frac{1}{2\pi} \int dk_x dk_y \mathrm{Tr}[\mathbf{A}_{\boldsymbol{n}}(k_x, k_y)], \tag{2}$$

where $\mathbf{A}_{\boldsymbol{n}}(k_x, k_y) = \langle \psi_n(\boldsymbol{k}) | i\partial_{\mathbf{k}} | \psi_n(\boldsymbol{k}) \rangle$ is the Berry connection, n represents the band index, the symbol $\partial_{\mathbf{k}}$ is a vector gradient operator in momentum space, and the integration is performed over the entire Brillouin zone (BZ). For a system with inversion symmetry, the calculation of $\mathbf{P}$ can be substantially simplified by checking the parities of eigenstates at the high-symmetry points in the BZ [43]:

$$P_m = \frac{1}{2}\left(\sum_n q_m^n \mathrm{mod} 2\right), \quad (-1)^{q_m^n} = \frac{\eta(X_m)}{\eta(\Gamma)}, \tag{3}$$

where the summation is taken over all the occupied bands, η denotes the parity associated with π rotation, and m stands for x or y. Equation (3) indicates that the topology of the current AC system is encoded in the parities of Bloch eigenstates at high-symmetry points. For example, the eigenstates calculated from finite-element simulation and the corresponding eigenvectors at the X point on the third branch for configurations A and B are shown in Fig. 1(b). It is easy to find that the parity η associated with π rotation is "$-$" for configuration A and "$+$" for configuration B. The difference in parity η implies that the topology of the two configurations is different because the topology depends on the way in which the unit cell is chosen [21,41,44,45]. By taking all eigenstates at the high-symmetry points into account, we obtain $P_A = (0, 0)$ and $P_B = (1/2, 1/2)$, which means that configuration A is trivial and B is nontrivial.

III. TWO TYPES OF CORNER STATES

Recently, it was found that in 2D systems the polarization (P_x, P_y) corresponds to the Wannier center of the Bloch state, which is the expectation value of the Wannier function in real space. The value of $P = p_x^2 + p_y^2$ indicates the distance of the Wannier center from the origin of a lattice site [13,14]. From a topological perspective, the mismatch of the Wannier center with the origin of a lattice site gives rise to a second-order boundary state at the corner of the system. These corner states are topologically nontrivial since they have the same origin as the end states in the 1D SSH model. In this

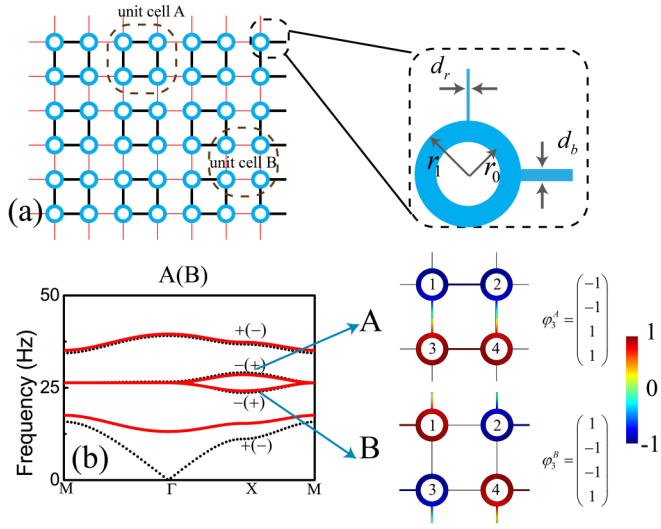

FIG. 1. (a) Schematic of the acoustic ring-waveguide system that can be described by the Hamiltonian model, i.e., Eq. (1). Each unit cell contains four identical hollow rings, whose inner and outer radii are fixed, connected by rectangular waveguides. Two different unit cells with inversed intercell and intracell hoppings are circled out. The hopping is characterized by the rectangular waveguides, whose width represents the hopping strength. (b) The calculated band structure using the finite-element method (black dots), compared with the results obtained from the tight-binding model (red line), where the fitting parameter is $\varepsilon_s = 26.375$, $w = 5$, $v = 1$, and all of the fitting parameters have the unit Hz. The symbol "±" means the parity of the states under π rotation, which is derived from the eigenfield distributions and eigenvectors shown in the right inset. Red (blue) in the right inset indicates the normalized maximum (minimum) acoustic pressure field, respectively.

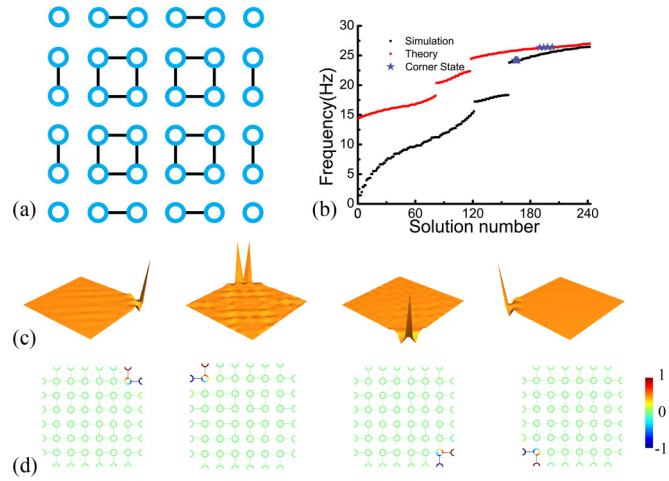

FIG. 2. The corner states in continuum. (a) Illustration of a 3×3 lattice with $w = 0$, where the corner states naturally appear. (b) The eigenmodes of a 10×10 sample calculated from both the tight-binding model (red point) and the numerical simulation result (black point). In the tight-binding model calculations, we introduce small random perturbations to all of the site energies and coupling parameters. The energy spectrum is plotted after an ensemble average of 10 configurations. The result shows four corner states in the bulk frequency region marked as purple stars. The field distribution of the four corner states from the tight-binding model and the finite-element simulation are shown in (c) and (d), respectively. The sample size we calculated in (d) is 3×3 for simplicity and clarity.

way, an analytically solvable tight-binding model with $w = 0$ (or $v = 0$) would offer direct insight for the existence of corner states. For a 2D system with $N \times N$ unit cells, as shown in Fig. 1(a), it corresponds to a topologically nontrivial phase with $w = 0$. Among all $4N^2$ sites of the system, there are $4N - 4$ dimers, $(N - 1)^2$ tetramers, and four isolated sites. Every dimer occupies energy $\varepsilon_s + v$ and $\varepsilon_s - v$. The tetramer occupies energy $\varepsilon_s \pm 2v$, and two degenerate energies ε_s. More interestingly, there are four isolated sites with energy ε_s, from which four corner states can be built. Here we want to point out that the energy of the corner state, ε_s, falls into the energy spectrum of the bulk tetramer states, which means that these corner states are embedded in the continuum. In contrast, if $v = 0$, the system is in the topologically trivial phase. There are N^2 bulk tetramer states, and no corner states are observed. Thus, we can conclude that the corner states only appear in a topologically nontrivial system.

Although the conditions of $w = 0$ or $v = 0$ are extreme, in the following we will show that the topological properties discussed earlier persist under more relaxed conditions, where neither w nor v is zero. For an $N \times N$ system with $w > v > 0$ (i.e., configuration A), there are $2N$ eigenstates with energy ε_s. We intentionally introduce small random perturbations in the hopping amplitudes and onsite energies to lift the degeneracy of these $2N$ states. We find that the randomly perturbed system has an energy spectrum that preserves the main features of the original periodic system, and no corner states are found. This is consistent with our previous analysis, since configuration A is topologically trivial. In contrast, configuration B ($v > w > 0$) can be adiabatically connected to the extreme case of $w = 0$, thus we expect that the corner states appear in the frequency range of bulk states. This is indeed verified by our calculations. In fact, even after we introduce random perturbations into configuration B (see details in Appendix C), we can still find four corner states with energy around ε_s. For a sample of configuration B with $N = 10$, we calculate the frequencies of the eigenstate by using both finite-element simulation and the tight-binding model, and the results are shown in Fig. 2(b). Both results confirm that the four corner states fall into the range of bulk state frequency. To the best of our knowledge, this is the first observation of nontrivial corner states in the continuum. The corresponding pressure field distributions given by both the tight-binding model and finite-element simulations are shown in Figs. 2(c) and 2(d), respectively.

In addition to the corner states found in a simple nontrivial system with configuration B, we also find another form of corner state in a more complex composite system consisting of a nontrivial sample surrounded by a trivial sample, as shown in Fig. 3(a). Here we simply set the width of the waveguides connecting the two systems d, representing intersystem hopping, to be identical to d_v, characterizing the intercell hopping in the nontrivial phase (configuration B), i.e., $d = d_v = 5$ cm. Four corner states are found at the interface between trivial and nontrivial phases. All of these four corner states are in the bulk gap region, which differs from the case shown in Fig. 2.

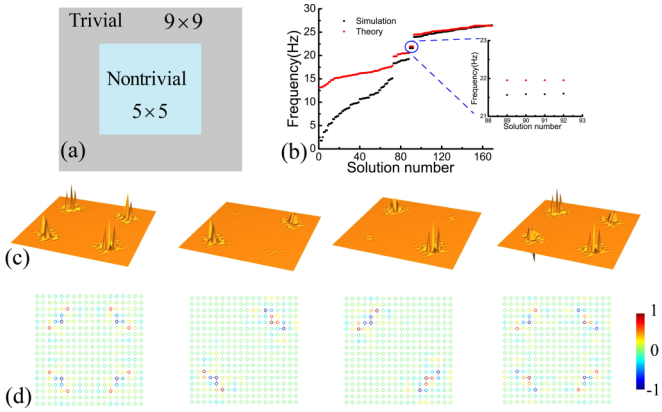

FIG. 3. The corner states in a gap of topological phononic clusters. (a) The sample consists of a topologically nontrivial system B surrounded by a topologically trivial system A. (b) The eigenmodes of the sample calculated from both the tight-binding model (red point) and the finite-element simulation result. We also set the coupling between systems A and B as $t = 5$. The result shows four corner states in the band-gap region. (c) and (d) The field distribution of the four corner states from the tight-binding model (c) and the finite-element simulation (d), respectively.

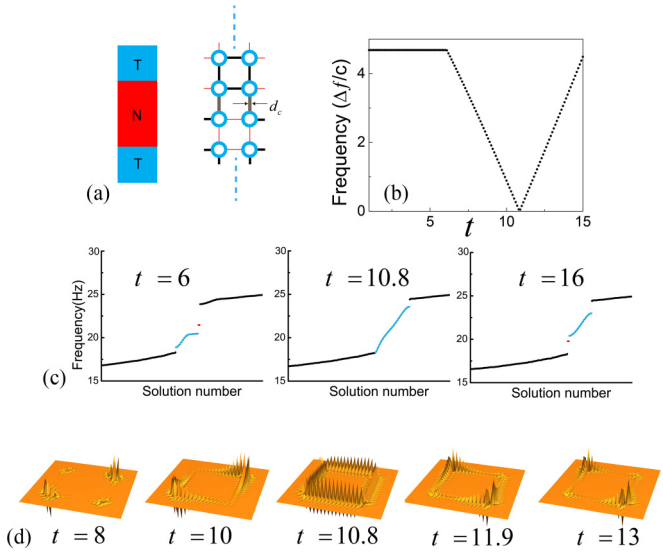

FIG. 4. The corner states evolution against intersystem hopping t. The sample consists of 27×27 unit cells. (a) The schematic of a structure that contains two interfaces between systems A and B, where the coupling parameters are undetermined. (b) The estimated band-gap size of the edge states as a function of hopping parameters t in the tight-binding model. The result indicates there would be a gapless edge state when $t = t_c = 10.8$. (c) The eigenfrequency spectrum of the sample when we change intersystem hopping t. The red points are corner states and the blue points are edge states. (d) The corner states delocalize when the gap of the edge states disappears at certain intersystem hopping $t = t_c = 10.8$.

The corresponding pressure field distributions for the corner states are obtained by using both the tight-binding model [Fig. 3(c)] and the finite-element simulations [Fig. 3(d)]. Both results confirm that the fields are highly localized around the four corners of the interface between the trivial and nontrivial phases.

The more interesting features of these four corner states are the delocalization and even the merging into edge states when the intersystem hopping (denoted as t in the tight-binding model) is tuned (details are available in Appendix D). When connecting configuration A with configuration B, we are endowed with some degree of freedom for selecting the intersystem hopping t(or the waveguide width d), as illustrated in Fig. 4(a). Different intersystem hopping leads to different configurations of the corner states, as demonstrated in Fig. 4(c). To determine the critical value of t (or d), one can take the following strategy by calculating the projected band structure of a ribbon structure consisting of a nontrivial sample sandwiched between two trivial samples with varying t. There always exists a band gap in the projected band structure except when $t = t_c = 10.8$, which, in our setup, corresponds to the waveguide width $d = d_c = 8.18$ cm in the full wave simulations (see details in Appendix D). From the tight-binding model, it is interesting to find that the size of the band gap depends linearly on $(t - t_c)$ when t deviates from t_c, as shown explicitly in Fig. 4(b). We show the energy spectrum and field distribution at $t = t_c = 10.8$ in the middle panels of Figs. 4(c) and 4(d), respectively, and we observe that the corner states merge into the edge state in this case. This is because the band gap vanishes at $t = t_c = 10.8$ and the corner states have to share the same energy with the edge states. In conjunction with the results presented in Fig. 3, this implies that the corner states are not determined solely by the bulk topological invariant, and in some cases they also depend crucially on the boundary conditions [23]. This finding indicates an effective way to manipulate the corner states by simply tuning the intersystem hopping. Figures 4(c) and 4(d) show the energy spectra and field distributions of corner states with different values of t. We observe that the corner states can stay below and isolated from the edge states, then merge into the edge states, and further stay above and isolated from the edge states, as the intersystem hopping t continuously increases.

IV. CONCLUSION

In conclusion, we find two types of nontrivial corner states in a second-order topological insulator, and interestingly, one type is identified as BIC, which means that they are perfectly confined without any radiation even when they lie inside the continuum and coexist with extended states. Both types of corner states are found to be associated with the nonzero dipole momentum in the bulk, in contrast with the quantized quadrupole momentum as reported in the literature. We develop a simple tight-binding model that can provide an analytic solution and direct insight into the origin of the corner states. Full wave simulations based on the realistic acoustic waveguide system are also presented, and together with the tight-binding model they corroborate the robustness of the corner states even when random perturbation is introduced. Our findings not only offer an experimentally feasible platform for the study of HOTI in classical wave systems, but they also provide an alternative method for the realization of BIC in a simple system. This may stimulate subsequent explorations

of the interesting interplay between BIC and HOTI as well as large-area high-power applications in acoustic waves.

ACKNOWLEDGMENTS

The work described here are supported by King Abdullah University of Science and Technology Office of Sponsored Research (OSR) under Award No. OSR-2016-CRG5-2950 and Baseline Research Fund BAS/1/1626-01-01, and by the National Natural Science Foundation of China (Grants No. 11274120 and 11574087).

APPENDIX A: THE FITTING PARAMETERS OF THE TIGHT-BINDING MODEL

To compare the results obtained from the tight-binding model and the full wave simulation, we need to know the values of various parameters such as the on-site energy. To determine these values, we let the frequencies of the eigenstates at the Γ point be identical. For the band structure shown in Fig. 1(b), we are interested in the second, third, fourth, and fifth branches. From the tight-binding model, we can get four eigenvalues of the Hamiltonian $H(k)$ [Eq. (1) in the main text] at the Γ point as a function of ε_s, w, and v. To be more precise, these functions are $\varepsilon_s + 2(w+v)$, ε_s, ε_s, $\varepsilon_s - 2(w+v)$, where $w = 5v$. We set $v = 1$ and $\varepsilon_s = 26.375$, such that the eigenfrequency on the second branch at the Γ point, $\varepsilon_s - 2(w+v)$, is equal to that calculated from the full wave simulation of a real acoustic model. We find that by using this set of fitting parameters, the tight-binding model can quantitatively reproduce the entire second, third, fourth, and fifth branches of the real acoustic model. Furthermore, in both models, the band topology is encoded in the parity of the eigenfunctions at the high symmetry point. We examine the parity of the eigenfunction calculated from both the tight-binding and the real model, and the results are consistent. An example taken at the X point is shown in Fig 1(b) in the main text.

APPENDIX B: "ZERO-COUPLING" CONDITION IN THE ACOUSTIC MODEL

As stated in the main text, the on-site energy and hopping amplitudes in the tight-binding model can be characterized by rings and waveguides in realistic acoustic waveguide systems. One interesting example is the corner states shown in Fig. 2(b), which are related to the "zero coupling" at the boundary between lattice sites and the "vacuum." The realization of zero coupling in the real acoustic system is not as obvious as that in the tight-binding model. Here we explain how to realize the condition of zero coupling at the sample boundary.

According to the analysis in the main text, there exist edge states at the boundary of a topologically nontrivial system, while no edge state emerges when the system is trivial. In this regard, we calculate the projected band structure of a supercell that contains 10 unit cells along the y direction and is periodically repeated along the x direction. The results predicted by the tight-binding model are shown in Figs. 5(a) and 5(b)), where the bulk topology is indicated by whether there exist edge states. For realistic acoustic waveguide systems, we consider the design of three different boundaries, as shown in Figs. 5(c)–5(h), respectively. We find that the edge states appear only for a type III boundary, and no edge state emerges for the other two types of boundaries. Thus, we conclude that the condition of "zero coupling" in the tight-binding model can be simulated by a type III boundary design in realistic acoustic systems.

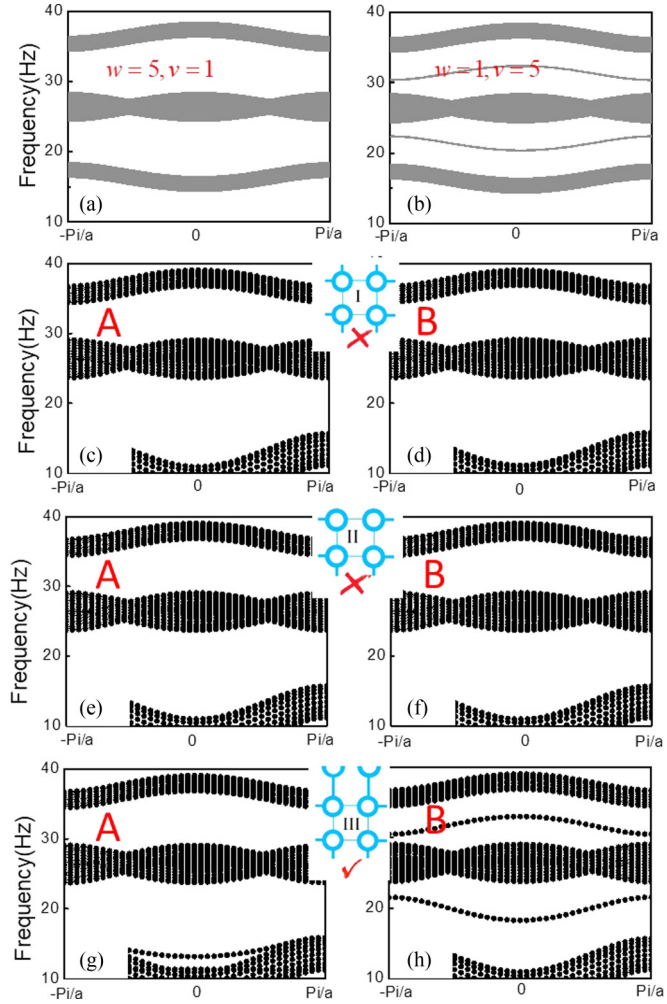

FIG. 5. The projected band structure from the tight-binding calculations [(a) and (b)] and full wave simulations [(c)–(h)]. Only the system with boundary type III exhibits an edge state predicted by the tight-binding model.

APPENDIX C: THE ROBUSTNESS OF THE CORNER STATE IN THE CONTINUUM

In the main text, we consider an extreme condition, i.e., $w = 0$, under which the corner states coexist with the continuum. In that situation, the system can be well-identified as dimers, tetramers, and isolated states, respectively. The corner states can be constructed from the isolated states and are robust. Then we consider a general topologically nontrivial system with nonzero w, and the energy spectrum of the corner states is fixed as ε_s. We note that many bulk states also take the energy ε_s, and the system has a high

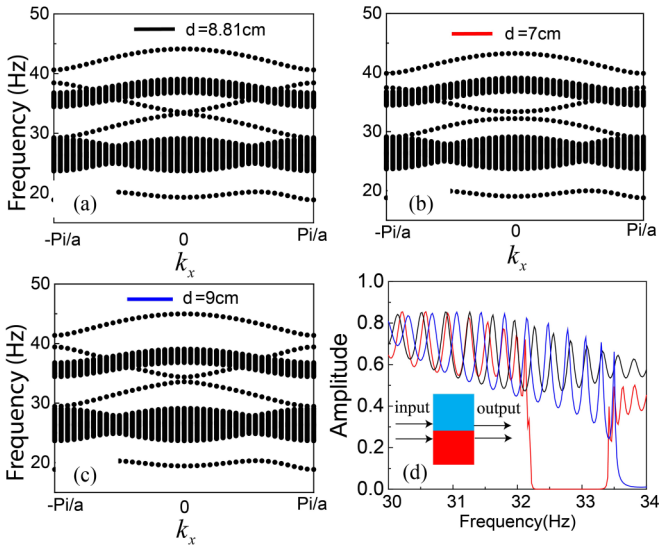

FIG. 6. Gapless edge state by tuning the width of the coupling waveguide. (a) The edge-state dispersion turns out to be gapless when we take $d = d_c = 8.18$ cm compared to the results in (b) $d = 7$ cm and (c) $d = 9$ cm. (d) The gapless behavior is also captured by measuring the amplitude of acoustic pressure in the output channel.

density of states at the energy ε_s, which makes the corner states indistinguishable compared with the bulk states. We introduce small random perturbations $\varepsilon_p \in (-0.1, 0.1)$ into all site energy to separate the corner states from the bulk states with energy ε_s. Then the corner states and the bulk states will take distinct eigenenergies. In the trivial case no corner state exists, while in the nontrivial case the corner state can be clearly observed as shown in Fig. 2(c). The corner states always exist in the continuum regime regardless of small perturbations, indicating that the corner states are robust and determined by the nontrivial bulk topology instead of a certain boundary.

APPENDIX D: THE GAPLESS EDGE STATES AND WAVE PROPAGATION

In this Appendix, we will discuss the dispersion of an edge state living between topologically trivial and nontrivial systems. Generally speaking, the edge-state dispersion is not

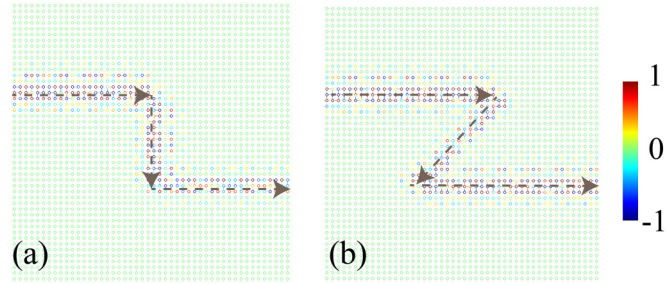

FIG. 7. The wave propagates along the interface between topological trivial system A and nontrivial system B. (a) The sample takes a boundary along the x and y directions. (b) The sample takes a boundary along x and the $x = y$ direction. The results show the wave propagation along the interface.

gapless. But we find that, by tuning the coupling parameters between trivial and nontrivial systems, the edge states can be gapless, as shown in Fig. 4(b). This is verified in the real acoustic model. We take the edge state in the second band gap as an example. We tune the width of the coupling waveguide and calculate the projected band structure. When $d = d_c = 8.18$ cm, closing to the value predicted by the tight-binding model, the edge state is gapless. The interface can be regarded as a waveguide at the frequency of interface states, and the gapless property of the interface state can be captured by measuring the transmittivity of the waveguide. When we take $d = 7$ or 9 cm, we can observe a frequency range of low transmission corresponding to a band-gap region. The results are consistent with the projected band structure shown in Fig. 6.

We also demonstrate the simulated wave propagation behavior along a specifically designed interface. The system contains 24×24 unit cells and is equally divided into systems A and B, noting that the interface does not break the rings in the unit cells. We consider two samples: the first sample, shown in Fig. 7(a), consists of boundaries along the x and y directions, while the second sample, illustrated in Fig. 7(b), introduces a boundary along the $x = y$ direction. A point source is put on the left boundary, while the acoustic wave is localized in the vicinity of the interface and decays exponentially into the bulk, indicating the existence of the interface state between these two insulating ACs.

[1] J. E. Moore, Nature (London) **464**, 194 (2010).
[2] M. Z. Hasan and C. L. Kane, Rev. Mod. Phys. **82**, 3045 (2010).
[3] X.-L. Qi and S.-C. Zhang, Rev. Mod. Phys. **83**, 1057 (2011).
[4] C. L. Kane and E. J. Mele, Phys. Rev. Lett. **95**, 226801 (2005).
[5] B. A. Bernevig, T. L. Hughes, and S.-C. Zhang, Science **314**, 1757 (2006).
[6] D. Xiao, W. Yao, and Q. Niu, Phys. Rev. Lett. **99**, 236809 (2007).
[7] K. F. Mak, K. L. McGill, J. Park, and P. L. McEuen, Science **344**, 1489 (2014).
[8] L. Fu, Phys. Rev. Lett. **106**, 106802 (2011).
[9] M. C. Rechtsman, J. M. Zeuner, Y. Plotnik, Y. Lumer, D. Podolsky, F. Dreisow, S. Nolte, M. Segev, and A. Szameit, Nature (London) **496**, 196 (2013).
[10] L. Lu, J. D. Joannopoulos, and M. Soljacic, Nat. Photon. **8**, 821 (2014).
[11] Z. Yang, F. Gao, X. Shi, X. Lin, Z. Gao, Y. Chong, and B. Zhang, Phys. Rev. Lett. **114**, 114301 (2015).
[12] C. He, X. Ni, H. Ge, X.-C. Sun, Y.-B. Chen, M.-H. Lu, X.-P. Liu, and Y.-F. Chen, Nat. Phys. **12**, 1124 (2016).
[13] W. A. Benalcazar, B. A. Bernevig, and T. L. Hughes, Science **357**, 61 (2017).
[14] Z. Song, Z. Fang, and C. Fang, Phys. Rev. Lett. **119**, 246402 (2017).

[15] J. Langbehn, Y. Peng, L. Trifunovic, F. von Oppen, and P. W. Brouwer, Phys. Rev. Lett. **119**, 246401 (2017).
[16] W. A. Benalcazar, B. A. Bernevig, and T. L. Hughes, Phys. Rev. B **96**, 245115 (2017).
[17] F. Schindler, A. M. Cook, M. G. Vergniory, Z. Wang, S. S. P. Parkin, B. A. Bernevig, and T. Neupert, Sci. Adv. **4**, eaat0346 (2018).
[18] M. Ezawa, Phys. Rev. Lett. **120**, 026801 (2018).
[19] C. W. Peterson, W. A. Benalcazar, T. L. Hughes, and G. Bahl, Nature (London) **555**, 346 (2018).
[20] S. Imhof *et al.*, Nat. Phys. **14**, 925 (2018).
[21] B.-Y. Xie, H.-F. Wang, H.-X. Wang, X.-Y. Zhu, J.-H. Jiang, M. H. Lu, and Y. F. Chen, Phys. Rev. B **98**, 205147 (2018).
[22] X. Zhang, H.-X. Wang, Z.-K. Lin, Y. Tian, B. Xie, M.-H. Lu, Y.-F. Chen, and J.-H. Jiang, Nat. Phys. **15**, 582 (2019).
[23] H. Xue, Y. Yang, F. Gao, Y. Chong, and B. Zhang, Nat. Mater. **18**, 108 (2019).
[24] X. Ni, M. Weiner, A. Alù, and A. B. Khanikaev, Nat. Mater. **18**, 113 (2019).
[25] M. Serra-Garcia, V. Peri, R. Süsstrunk, O. R. Bilal, T. Larsen, L. G. Villanueva, and S. D. Huber, Nature (London) **555**, 342 (2018).
[26] C. W. Hsu, B. Zhen, A. D. Stone, J. D. Joannopoulos, and M. Soljačić, Nat. Rev. Mater. **1**, 16048 (2016).
[27] J. Lee, B. Zhen, S.-L. Chua, W. Qiu, J. D. Joannopoulos, M. Soljačić, and O. Shapira, Phys. Rev. Lett. **109**, 067401 (2012).
[28] M. Robnik, J. Phys. A **19**, 3845 (1986).
[29] H. Friedrich and D. Wintgen, Phys. Rev. A **32**, 3231 (1985).
[30] F. Remacle, M. Munster, V. B. Pavlov-Verevkin, and M. Desouter-Lecomte, Phys. Lett. A **145**, 265 (1990).
[31] K. Hirose, Y. Liang, Y. Kurosaka, A. Watanabe, T. Sugiyama, and S. Noda, Nat. Photon. **8**, 406 (2014).
[32] M. Meier, A. Mekis, A. Dodabalapur, A. Timko, R. E. Slusher, J. D. Joannopoulos, and O. Nalamasu, Appl. Phys. Lett. **74**, 7 (1999).
[33] S. Noda, M. Yokoyama, M. Imada, A. Chutinan, and M. Mochizuki, Science **293**, 1123 (2001).
[34] A. A. Yanik, A. E. Cetin, M. Huang, A. Artar, S. H. Mousavi, A. Khanikaev, J. H. Connor, G. Shvets, and H. Altug, Proc. Natl. Acad. Sci. (USA) **108**, 11784 (2011).
[35] B. Zhen, S.-L. Chua, J. Lee, A. W. Rodriguez, X. Liang, S. G. Johnson, J. D. Joannopoulos, M. Soljačić, and O. Shapira, Proc. Natl. Acad. Sci. (USA) **110**, 13711 (2013).
[36] J. M. Foley, S. M. Young, and J. D. Phillips, Phys. Rev. B **89**, 165111 (2014).
[37] Y. Yang, Z. Yang, and B. Zhang, J. Appl. Phys. **123**, 091713 (2018).
[38] Z.-G. Chen and Y. Wu, Phys. Rev. Appl. **5**, 054021 (2016).
[39] Z.-G. Chen, J. Zhao, J. Mei, and Y. Wu, Sci. Rep. **7**, 15005 (2017).
[40] C. Kittel, *Introduction to Solid State Physics* (Wiley, New York, 2004).
[41] F. Liu and K. Wakabayashi, Phys. Rev. Lett. **118**, 076803 (2017).
[42] R. Resta, Rev. Mod. Phys. **66**, 899 (1994).
[43] C. Fang, M. J. Gilbert, and B. A. Bernevig, Phys. Rev. B **86**, 115112 (2012).
[44] M. Xiao, G. Ma, Z. Yang, P. Sheng, Z. Q. Zhang, and C. T. Chan, Nat. Phys. **11**, 240 (2015).
[45] K. H. Choi, C. W. Ling, K. F. Lee, Y. H. Tsang, and K. H. Fung, Opt. Lett. **41**, 1644 (2016).